Description of HFO-1234yf with BACKONE equation of state

Ngoc Anh Lai[a,*], Jadran Vrabec[b], Gabriele Raabe[c], Johann Fischer[d], Martin Wendland[d]

[a] Heat Engineering Department, Institute of Heat Engineering and Refrigeration, Hanoi University of Science and Technology, Hanoi, Vietnam;

[b] Thermodynamik und Energietechnik , Universität Paderborn, 33098 Paderborn, Germany;

[c] Institut für Thermodynamik, Technische Universität Braunschweig, 38106 Braunschweig, Germany;

[d] Institut für Verfahrens- und Energietechnik, Universität für Bodenkultur, A-1190 Wien, Austria.

Abstract

The hydrofluoroolefin 2,3,3,3,-tetrafluoroprop-1-ene (HFO-1234yf) is a refrigerant with a low global warming potential that can be used as a working fluid in refrigeration cycles, heat pumps, and organic Rankine cycles (ORC). This paper aims to accurately describe the thermodynamic properties of HFO-1234yf with the molecular based BACKONE equation of state (EOS). The BACKONE parameters are fitted to experimental vapour pressures and saturated liquid densities. For the ideal gas heat capacities very recent experimental results are taken. For the data used in the fit, the uncertainties of calculated values from the BACKONE EOS are 0.36% for vapour pressures and 0.37% for saturated liquid densities. For predicted data, the uncertainties of calculated values from the BACKONE EOS are 0.29% for liquid densities and 0.99% for pressures in the gas phase. Predicted isobaric heat capacities in the liquid are within the experimental uncertainties of ± 5%. Comparisons with the results from the extended corresponding state (ECS) model and with recent molecular simulation data confirm the high quality of the BACKONE EOS.

Keywords: 2,3,3,3,-tetrafluoroprop-1-ene (HFO-1234yf), equation of state (EOS), working fluid, refrigeration cycle, organic Rankine cycle (ORC)

[*] Corresponding author. Tel: +84 982051144, Fax. +84 43 8683634, Email: anhngoclai@yahoo.com

1. Introduction

The European Union issued a f-gas regulation [1] and a directive [2] that bans fluorinated greenhouse gases having global warming potentials (GWP) greater than 150 in new car models from January 1, 2011 and in all new vehicles from January 1, 2017. The US Environmental Protection Agency (EPA) has recently released a proposed rule for HFO-1234yf as an automotive refrigerant [3]. According to EPA, HFO-1234yf has a 100 year direct GWP of 4 and an ozone depletion potential (ODP) of zero [4]. According to DuPont and Honeywell, the life cycle climate performance (LCCP) of HFO-1234yf is the lowest one [5]. In terms of safety, HFO-1234yf has a low acute and chronic toxicity [5]. HFO-1234yf has a relatively high lower flammability limit, high minimum ignition energy, and very low burning velocity [6]. Furthermore, HFO-1234yf has a high auto-ignition temperature of 678.15 K [7]. Regarding flammability, the classification is not yet harmonized [8, 9]. In the German version of the materials safety data sheet corresponding to EC-rules, Honeywell states that HFO-1234yf is “hochentzündlich” (highly flammable) [8], whereas in the final report to EPA, Honeywell and Dupont state that HFO-1234yf is mildly flammable [9]. This disagreement should be clarified. In the research of Minor et al. of Dupont [6], HFO-1234yf is stated to be safe for use as a refrigerant in vehicles [6]. However, another safety issue for the use of HFO-1234yf as automotive refrigerant is the HF production after contact with hot surfaces for leaking air conditioning systems [10].

HFO-1234yf is applicable not only in refrigeration cycles but also in Clausius–Rankine cycles and triangular cycles. In order to study the replacement of phased out refrigerants by HFO-1234yf on the basis of numerical simulations of thermodynamic cycles, its thermodynamic properties are needed. Different experimental studies on the thermodynamic behaviour of HFO-1234yf have been carried out [11 - 17]. These studies provide important data for the construction of equations of state (EOS) for the calculation of a variety of thermodynamic properties. These data were used for the determination of parameters of various EOS. These are the cubic Peng-Robinson EOS [18, 19], the Martin-Hou EOS [12], the Patel–Teja EOS [20] and the extended

corresponding state (ECS) model [20] based on [21], as well as the short multiparameter EOS [22] of the Span–Wagner type [23, 24].

It is well-known that multiparameter EOS are the most accurate type provided that for their construction sufficient accurate experimental data are available for a large region of the fluid state. If the number of experimental data is at least moderate, short multiparameter EOS of the Span–Wagner type [24] or other types of EOS can be used. Otherwise, multiparameter EOS should not be used. The ECS model requires a reliable EOS for a suitable reference fluid that is guaranteed in [20] by [21]. However, the extension of ECS and multiparameter EOS to mixtures is still very challenging. Regarding other EOS, Akasaka et al. [20] have shown that the Peng–Robinson [19] and the Patel–Teja EOS are not very accurate for HFO-1234yf. Promising types of molecular based EOS, such as BACKONE [25, 26] and PC-SAFT [27], have not been applied to HFO-1234yf prior to this work. Molecular based EOS have only between three and five substance specific parameters that can be fitted to vapour pressures and saturated densities only. These EOS are particularly suitable for fluids with a limited or moderate number of available experimental data. Furthermore, they can easily be extended to mixtures with only one additional parameter for each binary.

The BACKONE EOS was developed for compact molecules so that it is better suited in such cases than the PC-SAFT EOS, which was rather aimed at chain like molecules [28, 29]. The BACKONE EOS has been successfully applied to different pure and mixed working fluids regarding different applications [30-37]. Because HFO-1234yf is a compact molecule, the BACKONE EOS was chosen in this study.

In the following Sections, the BACKONE parameters for HFO-1234yf will be optimized to experimental data of vapour pressures and saturated liquid densities. Then thermodynamic quantities resulting from BACKONE will be compared with experimental data as well as with results from the ECS approach [20] and molecular simulation data [38].

2. Available thermodynamic data

In Subsection 2.1., available experimental data with the exception of isobaric ideal gas heat capacities c_p^0 are compiled. In Subsection 2.2., experimental c_p^0 data are discussed in comparison with quantum mechanical results.

2.1. Experimental data

Table 1 presents experimental data for the critical temperature T_c, the critical pressure p_c, and the critical density ρ_c. It shows that the published critical data from Tanaka and Higashi [11], Leck [12] and Nicola et al. [13] are almost identical throughout. The differences among them are negligible for each quantity. Tanaka and Higashi have carried out a series of measurements over a large part of the fluid region, which are important for the present parameterisation of the BACKONE EOS. Thus, for consistency, the critical data from Tanaka and Higashi [11] were chosen as reference.

In Table 2, experimental data for vapour pressure of HFO-1234yf from different sources [11, 14, 16] are compiled. In order to decide which data should be used in the construction of the BACKONE EOS for HFO-1234yf, the Wagner equation [39] was fitted to all experimental data from the three sources [11, 14, 16]. A comparison between experimental data and the values from the Wagner equation shows that experimental data from Hulse [14] exhibit large deviations and are not consistent with those from Tanaka and Higashi [11] and Nicola et al. [16]. Almost all currently available EOS for HFO-1234yf are based on the experimental data from Tanaka and Higashi [11] and Nicola et al. [16] and compare with it. In this study, vapour pressure data from Tanaka and Higashi [11] and Nicola et al. [16] were taken for the parameterization of the BACKONE EOS.

Table 3 contains information on the experimental data for the saturated liquid densities ρ' together with temperature ranges, density ranges, experimental uncertainties, numbers of data points, and sources for the experimental data. The ρ' values of Tanaka and Higashi [11] and the data of Hulse et al. [14] were tested with one-parameter and two-parameter equations for

saturated liquid density of [40]. It was found that both data sources are consistent and both of them were used here.

In the construction of the BACKONE EOS for HFO-1234yf, the BACKONE parameters were fitted to vapour pressures and saturated liquid densities. In order to assess the predictive power of the BACKONE EOS, experimental pvT data in the liquid and the vapour phase, cf. Table 4, isobaric heat capacity data of the liquid, cf. Table 5, and enthalpy data at saturation lines, cf. Table 6 were used. Figure 1 shows the distribution of pvT data taken for this study from Nicola et al. [13] and Tanaka et al. [15]. But note that only data on the saturation line were used for fitting.

2.2. Ideal gas heat capacities

The calculation of caloric properties with the BACKONE EOS requires additional information on the isobaric ideal gas heat capacity c_p^0. Very recently, experimental data for c_p^0 were published [41]. These were measured with the acoustic resonance method in a spherical cavity in the temperature range from 278.15 K to 353.15 K. Moreover, there are three sources [12, 14, 43] presenting ideal gas heat capacities from quantum mechanical calculations. Hulse et al. [14] give c_p^0 values from 213.15 K to 573.15 K that were calculated as outlined by Rowley [42]. Leck [12] calculated ideal gas heat capacity data by *ab-initio* molecular orbital methods using the “Gaussian-03” software (CyberChem Inc.). The results are given in polynomial form, without a statement on the temperature range. Finally, Raabe and Maginn [43] reported results for six temperatures in the range from 273.15 K to 310 K and described their methodology in detail. A comparison of the results from all sources at some temperatures is given in Table 7. Comparing with the experimental data, the results of Hulse et al. are higher by about 1.1 %, the results of Leck are lower by about 2.6%, and the results of Raabe and Maginn are lower by about 10%. The results of Hulse et al. [14] and Leck [12] just bracket the experimental data and hence the latter [41] were taken for subsequent calculations.

3. BACKONE parameters and comparison with experimental results

First, a short description of the BACKONE EOS is briefly presented for the convenience of the reader. In fact, BACKONE is a family of physically based EOS. BACKONE writes the Helmholtz energy in terms of a sum of contributions from characteristic intermolecular interactions [25] as $F = F_H + F_A + F_D + F_Q$, where F_H is the repulsive hard-body contribution, F_A is the attractive dispersion contribution, F_D is the dipolar contribution, and F_Q is the quadrupolar contribution. The general parameters of the BACKONE contributions F_H, F_A, F_D, and F_Q were given in [25, 26]. The molecular based BACKONE EOS contains up to five substance specific parameters, i.e.: characteristic temperature T_0, characteristic density ρ_0, anisotropy factor α, reduced dipolar moment μ^{*2}, and reduced quadrupolar moment Q^{*2}. Depending on the molecular structure of the fluid, BACKONE has three to five parameters that are fitted to vapour pressures and saturated densities.

In this study, the BACKONE EOS was fitted to vapour pressure data from Tanaka and Higashi [11] and Nicola et al. [16] and saturated liquid densities from Tanaka and Higsahi [11] and Hulse et al. [14]. The fitting ranges were 0.0389 MPa to 3.2184 MPa for pressure and 224.13 K to 365.93 K for temperature. First, the BACKONE EOS was fitted with only 4 parameters, excluding the dipole moment contribution. Second, the BACKONE EOS was fitted with all 5 parameters. The comparison of the 4-parameter EOS and the 5-parameter EOS is given in Table 8. This Table does not include caloric data, because the experimental values are strongly scattered as discussed below. Table 8 shows that the contribution of the dipole moment is small. The differences in the average absolute deviation (AAD) of the thermodynamic properties between the 4-parameter and the 5-parameter model are negligible. Thus, the 4-parameter model was used in the following.

Figure 2 shows that the relative deviations between BACKONE vapour pressures and experimental data from Tanaka and Higashi [11] and Nicola et al. [16] are mostly within 0.5%. The AAD between BACKONE vapour pressures and experimental data from Tanaka and Higashi [11] and Nicola et al. [16] are 0.36%. In particular, the AAD is 0.30% for the data of

Tanaka and Higashi [11] and 0.38% for the data of Nicola et al. [16]. For comparison, the AAD of the ECS model [20] is 0.18% for the data from [11] and 0.28% for the data from [16]. In view of the fact that for the larger data set of Nicola et al. [16] the uncertainties were estimated by the authors to be 0.25%, both BACKONE and ECS yield a very satisfying agreement, where the performance of ECS is somewhat better.

Similar to the AAD for the vapour pressures, the overall AAD for the BACKONE saturated liquid densities from the fitted experimental data of Tanaka and Higashi [11] and Hulse et al. [14] is 0.37%. In particular, the AAD is 0.29% for data of Tanaka and Higashi [11] and 0.40% for data of Hulse et al. [14]. Figure 3 shows the relative deviations between the saturated liquid densities from BACKONE and experimental data.

Summarizing, the AADs between BACKONE results and experimental vapour pressures and saturated liquid densities are smaller than 0.37%. This shows that the BACKONE EOS can well fit the experimental data. In order to evaluate the predictive power of the BACKONE EOS, its results are compared in the following with experimental data that were not used in the fitting procedure. First, we present the critical data from BACKONE, which were obtained as $T_{c,\,B1}$ = 372.596 K, $p_{c,\,B1}$ = 3.6249 MPa, and $\rho_{c,\,B1}$ = 3.9554 mol/dm^3 and have to be compared with the experimental data from [11] in Table 1. It can be seen that the BACKONE critical temperature $T_{c,B1}$ is only 1.3% higher than the experimental value, which is a rather small deviation. As a consequence of the higher $T_{c,B1}$ the BACKONE critical pressure is higher than the experimental value and the BACKONE critical density is lower than the experimental value, as the vapour pressures and the saturated liquid densities of BACKONE are very close to the experimental values at given subcritical temperatures.

Next, Figure 4 shows BACKONE predictions for pvT data in the homogeneous liquid in comparison with the experimental data of Tanaka et al. [15]. The relative deviations between BACKONE liquid densities and experimental data are mostly from -0.5% to -0.1% with the exception of two data points. The AAD for all 23 data points is 0.29%, which is the same deviation as obtained for the saturated liquid densities to which BACKONE was fitted. For

comparison, the AAD of the liquid densities of the ECS model [20] was given as 0.56%. Hence, for the liquid densities BACKONE shows a better performance than ECS.

Figure 5 shows BACKONE predictions of pressures in the homogeneous vapour in comparison with the experimental pvT data of Nicola et al. [13] at different densities. It can be seen that the relative deviations between predicted and experimental pressures are mostly from -1.5% to 0.0%. The AAD for all 136 data points is 0.99%, whilst the experimental uncertainties were estimated to be less than 0.8% [13].

For completeness, the BACKONE results were compared to experimental caloric data that were not used in fitting the BACKONE parameters and hence were also predicted values.

First, the enthalpies of vapourization Δh from BACKONE were compared with experimental values from Spatz and Minor [17]. The enthalpy of vapourization was obtained as the difference of the enthalpy of the saturated vapour h" and the enthalpy of the saturated liquid h' at the same temperature and pressure as $\Delta h = h" - h'$. This means that a) the reference state point of the enthalpy and b) the isobaric ideal gas heat capacity cancel out. The comparison in Fig. 6 shows that Δh values from BACKONE are a smooth function of the temperature and are higher than the experimental values from [17] which are scattered. The average difference is 0.47 kJ/mol with a minimum deviation of 0.24 kJ/mol at 303.75 K (p = 0.8 MPa) and a maximum deviation of 0.74 kJ/mol at 342.18 K (p = 2.0 MPa).

Finally, Table 9 shows a comparison between calculated and experimental [15] isobaric heat capacities c_p in the liquid. The calculated values are based on BACKONE using the experimental isobaric ideal gas heat capacities c_p^0 from Kano et al. [41]. The Table also contains the c_p^0 values in order to demonstrate the ideal gas and the residual contributions. First, it can be seen that the experimental values are scattered and have very low uncertainties. Next we see that the calculated values are all within the experimental uncertainties.

4. Thermodynamic data of HFO-1234yf from BACKONE

For the convenience of the reader, Tables 10 and 11 present data in the homogeneous and two phase region obtained from BACKONE. The data in these Tables were generated with a reference enthalpy h_0 = 0.0 J/mol and reference entropy s_0 = 0.0 J/mol K for the saturated liquid at the normal boiling point (T = 243.74 K).

Table 10 contains vapour pressures, saturated densities, saturated enthalpies, and saturated entropies as a function of temperature. Table 11 includes temperature and pressure based properties, such as enthalpy, entropy, and specific volume. The thermodynamic properties of HFO-1234yf from the BACKONE EOS are also graphically shown in Fig. 7. Note that the saturated vapour curve of HFO-1234yf is nearly vertical, which has advantages for using it as a working fluid in refrigeration cycles [30-36] or organic Rankine cycles [37, 44].

5. Comparison with molecular simulation results

Raabe and Maginn [38, 43] have recently developed a force field for HFO-1234yf, which is an atomistic model with partial electric charges. With that model, they calculated thermodynamic saturation properties by Gibbs Ensemble Monte Carlo simulations. Table 12 shows vapour pressures, saturated densities, and enthalpies of vaporization from simulation and BACKONE in the temperature range from $0.66 < T/T_c < 0.93$. The uncertainties of the simulation data are also contained in Table 12.

The comparison in Table 12 shows that most simulation data with their uncertainties bracket the BACKONE results. Exceptions are the vapour pressure at 333.15 K and the enthalpies of vapourization from 244 K to 313.15 K, which are too high. This indicates that the atomistic model is in principle rather good, especially when taking into account that the force field was not exclusively optimized to predict the properties of HFO-1234yf only, but to yield predictions for a group of fluoropropene refrigerants [43]. The problem, however, are the large simulation uncertainties. Of course, one might think of increasing the length of the simulation runs to lower the simulation uncertainties. More fundamental considerations, however, should

deal with the simulation methodology, as it seems that the NpT+ test particle method yields results with less scatter [45-48].

6. Summary and Conclusions

Thermodynamic data of HFO-1234yf were modelled with the BACKONE EOS. It was shown that the BACKONE EOS is not only good for describing data, but also good for predictions. In detail, for fitted data, the uncertainties of calculated values from the BACKONE EOS are 0.36% for vapour pressures using two experimental sources [11, 16] and 0.37% for saturated liquid densities using the experimental data of Tanaka and Higashi [11] and Hulse et al. [14]. With respect to predictions, the uncertainties of calculated values from the BACKONE EOS are 0.29% for liquid densities [15] and 0.99% for pressures in the gas phase [16]. Predicted isobaric heat capacities in the liquid are within the experimental uncertainties [15], whilst the enthalpies of vapourization from BACKONE are on average higher by 0.47 kJ/mol than the strongly scattering experimental data [17].

In comparison with simulation data from the Gibbs Ensemble Monte Carlo method [38, 43], it was found that the atomistic model is rather good but the simulation uncertainties are quite large.

In further applications one can use the description of HFO-1234yf by the BACKONE EOS for modelling refrigeration cycles [31-36] and organic Rankine cycles [37, 44]. Finally, we want to emphasize that BACKONE has already been used successfully for the description of numerous mixtures [26, 31, 32, 35] so that blends containing HFO-1234yf may straightforwardly be described.

Nomenclature

AAD	Average absolute deviation
B1	BACKONE
c	Heat capacity (J/mol K)
ECS	Extended corresponding state

EOS	Equation of state
EPA	The U.S Environmental Protection Agency
F	Helmholtz energy
FA	Attractive dispersion force contributions to F
FD	Dipolar contribution to F
FH	Hard-body contribution to F
FQ	Quadrupolar contribution to F
GWP	Global warming potential
h	Enthalpy (J/mol)
HFO-1234yf	2,3,3,3,-tetrafluoroprop-1-ene
LCCP	Life cycle climate performance
MS	Molecular simulations
ODP	Ozone depletion potential
ORC	Organic Rankine cycle
p	Pressure (MPa)
Q^{*2}	Reduced squared quadrupolar moment
s	Entropy (J/mol K)
T	Temperature (K)
v	Specific volume (dm^3/mol)

Greek symbols

α	Anisotropy factor
ρ	Density (mol/dm^3)
μ^{*2}	Reduced squared dipolar moment

Subscripts

max	Maximum
min	Minimum
c	Critical
p	Isobaric
0	Characteristic
exp	Experiment
cal	Calculation

Superscripts

0	Ideal
’	Saturated liquid
”	Saturated vapour

Acknowledgements

One of the authors, Ngoc Anh Lai, gratefully acknowledges financial support by the Vietnamese National Foundation for Science and Technology Development (NAFOSTED).

References

[1] Regulation (EC) No 842/2006 of The European Parliament and of the Council of 17 May 2006 on certain fluorinated greenhouse gases, 2006. Official Journal of the European Union. Retrieved in December 2010 at: http://eur-lex.europa.eu/LexUriServ/LexUriServ.do?uri=OJ:L:2006:161:0001:0011:EN:PDF.

[2] Directive 2006/40/EC of The European Parliament and of the Council of 17 May 2006 relating to emissions from air-conditioning systems in motor vehicles and amending Council Directive 70/156/EC, 2006. Official Journal of the European Union. Retrieved in December 2010 at: http://eur-lex.europa.eu/LexUriServ/LexUriServ.do?uri=OJ:L:2006:161:0012:0018:EN:PDF.

[3] EPA, a proposed rule for HFO-1234yf as an automotive refrigerant. Retrieved in December 2010 at: http://www.gpo.gov/fdsys/pkg/FR-2009-10-19/pdf/E9-25106.pdf.

[4] EPA, Transitioning to low-GWP alternatives in unitary air conditioning, U.S. Environmental Protection Agency, U.S. Environmental Protection Agency, October 2010. Retrieved in December 2010 at: http://www.epa.gov/ozone/downloads/EPA_HFC_UAC.pdf.

[5] D. P. Wilson, M. Koban, HFO-1234yf Industry Update, February 6, 2009. Retrieved in December 2010 at: http://www.epa.gov/cpd/mac/Final%20EPA%20HFO-1234yf%20Coml%20Mtg_2_6_09,%20Modified%20Version.pdf.

[6] B. H. Minor, D. Herrmann, R. Gravell, Process Safety Progress, 29 (2010) 150-154.

[7] Honeywell, material safety data sheet for 2,3,3,3-Tetrafluoropropene (HFO-1234yf), Version 1, October 2008. Retrieved in December 2010 at: http://www.1234facts.com/pdf/HFO-1234yf%2011-10-08.pdf.

[8] Honeywell, Sicherheitsdatenblatt, 2,3,3,3-Tetrafluorprop-1-en, HFO-1234yf, printed: 17.10.2008. Retrieved in December 2010 at: http://www51.honeywell.com/sm/lgwp-de/common/documents/msds-documents/FP_LGWP_DE_HFO-1234yf_de_MSDS.pdf.

[9] D. P. Wilson, M. Koban, HFO-1234yf Industry Update, reported by Honeywell and Dupont to EPA, February 2009. Retrieved in December 2010 at: http://www.epa.gov/cpd/mac/Final%20EPA%20HFO-1234yf%20Coml%20Mtg_2_6_09,%20Modified%20Version.pdf.

[10] K. Holtappels, V. Schröder, G. Hoffmann, W. Plehn, SAE international. Retrieved in December 2010 at: http://www.sae.org/events/aars/presentations/2010/T7.pdf.

[11] K. Tanaka, Y. Higashi, Int. J. Refrigeration 33 (2010) 474-479.

[12] T. J. Leck, Proc. of 3rd IIR Conference on Thermophysical Properties and Transfer Processes of Refrigerants, Boulder, CO, USA, (2009).

[13] C. Di Nicola, G. Di Nicola, M. Pacetti, F. Polonara, G. Santori, J. Chem. Eng. Data 55 (2010) 3302-3306.

[14] R. Hulse, R. Singh, H. Pham, Proc. of 3rd IIR Conference on Thermophysical Properties and Transfer Processes of Refrigerants, Boulder, CO, USA, 2009.

[15] K. Tanaka, Y. Higashi, R. Akasaka, J. Chem. Eng. Data 55 (2010) 901-903.

[16] G. Di Nicola, F. Polonara, G. Santori, J. Chem. Eng. Data 55 (2010) 201–204.

[17] M. Spatz, B. Minor, Proceedings of the International Refrigeration and Air Conditioning Conference at Purdue, West Lafayette, Indiana, USA, 2008.

[18] J. S. Brown, C. Zilio, A. Cavallini, 3rd IIR Conference on Thermophysical Properties and Transfer Processes of Refrigerants, Boulder, CO, 2009.

[19] J. S. Brown, C. Zilio, A. Cavalini, Int. J. Refrigeration 33 (2010), 235-241.

[20] R. Akasaka, K. Tanaka, Y. Higashi, Int. J. Refrigeration 33 (2010) 52-60.

[21] R. Tillner-Roth, H. D. Baehr, Phys. Chem. Ref. Data 23 (1994) 657–729.

[22] R. Akasaka, Y. Kayukawa, Y. Kano, K. Fujii, International Symposium on Next-generation Air Conditioning and Refrigeration Technology, Tokyo, Japan, 2010.

[23] R. Span, W. Wagner, Int. J. Thermophys. 24 (2003) 1–39.

[24] E. W. Lemmon, R. Span, J. Chem. Eng. Data 51 (2006) 785–850.

[25] A. Müller, J. Winkelmann, J. Fischer, AIChE J. 42 (1996) 1116-1126.

[26] U. Weingerl, M. Wendland, J. Fischer, A. Müller, J. Winkelmann, AIChE J. 47 (2001) 705-717.

[27] J. Gross and G. Sadowski, Ind. Eng. Chem. Res. 40 (2001) 1244-1260.

[28] N. A. Lai, Thermodynamic data of working fluids for energy engineering, PhD thesis, University of Natural Resources and Life Sciences, Vienna, Austria, 2009.

[29] F. Castro-Marcano, C. G. Olivera-Fuentes, C. M. Colina, Ind. Eng. Chem. Res. 47 (2008) 8894–8905.

[30] S. Calero, M. Wendland, J. Fischer, Fluid Phase Equilib. 152 (1998) 1-22.

[31] U. Weingerl, M. Wendland, Proc. 20th International Conference of Refrigeration, IIR/IIF, Sidney, 1999.

[32] M. Wendland, S. Calero, U. Weingerl, J. Fischer, Chemie-Ingenieur-Technik 72 (2000) 738-742.

[33] B. Saleh, U. Weingerl, M. Wendland, Proc. IIR Conf. Thermophys. Properties and Transfer Processes of New Refrigerants, Paderborn 2001.

[34] B. Saleh, M. Wendland, Proc. Eurotherm Seminar 72 Thermodynamics, Heat and Mass Transfer of Refrigeration Machines and Heat Pumps, Valencia 2003.

[35] M. Wendland, B. Saleh, J. Fischer, Energy and Fuels 18 (2004) 938-951.

[36] B. Saleh and M. Wendland, Int. J. Refrigeration 29 (2006) 260-269.

[37] N. A. Lai, M. Wendland, J. Fischer, Energy 36 (2011) 199-211.

[38] G. Raabe, E. J. Maginn, J. Phys. Chem. Lett. 1 (2010) 93-96.

[39] W. Wagner, Cryogenics 13 (1973) 470-482.

[40] N. A. Lai, M. Wendland, J. Fischer, Fluid Phase Equilib. 280 (2009) 30–34.

[41] Y. Kano, Y. Kayukawa, K. Fujii, Int. J. Thermophys. 31 (2010) 2051–2058.

[42] R. L. Rowley, Statistical Mechanics for Thermophysical Property Calculations. Prentice Hall, 1994.

[43] G. Raabe, E. J. Maginn, J. Phys. Chem. B 114 (2010) 10133-10142.

[44] B. Saleh, G. Koglbauer, M. Wendland, J. Fischer, Energy 32 (2007) 1210-1221.

[45] D. Möller, J. Fischer, Molec. Phys. 69 (1990) 463-473, see also Erratum, Molec. Phys. 75 (1992) 1461–1462.

[46] D. Möller, J. Fischer, Fluid Phase Equilib. 100 (1994) 35-61.

[47] J. Stoll, J. Vrabec, H. Hasse, Fluid Phase Equilib. 209 (2003) 29-53.

[48] J. Stoll, J. Vrabec, H. Hasse, J. Chem. Phys. 119 (2003) 11396-11407.

Figure Captions

Figure 1. pvT data of HFO-1234yf used for fitting (—) and for evaluating the predictive power of the BACKONE EOS: ∇ liquid phase [15], o vapour phase [13].

Figure 2. Deviation of BACKONE vapour pressures for HFO-1234yf from experimental data of ▲ Tanaka and Higashi [11] and ● Nicola et al. [16].

Figure 3. Deviation of BACKONE saturated liquid densities for HFO-1234yf from experimental data of ▲ Tanaka and Higashi [11] and ● Hulse et al. [14].

Figure 4. Deviations of BACKONE liquid pvT data from experimental data of Tanaka et al. [15] at ● 310 K, ▲ 320 K, ○ 330 K, ∆ 340 K, ■ 350 K, and □ 360 K.

Figure 5. Deviations of BACKONE pressures in the vapour from experimental pvT data of Nicola et al. [13] at ◊ 0.044 mol/l, ■ 0.19 mol/l, □ 0.24 mol/l, ∆ 0.39 mol/l, ▲ 0.76 mol/l, ○ 1.27 mol/l, and ● 3.98 mol/l.

Figure 6. Enthalpies of vapourization: —— BACKONE, • experiment [17]. The temperatures T in the figure were obtained from the saturated vapour pressures p_s given in [17] via BACKONE.

Figure 7. Temperature - entropy diagram of HFO-1234yf from the BACKONE EOS, showing the saturated liquid and the saturated vapour curves and several isobars and isochors. The reference point: h = 0.0 J/mol, s = 0.0 J/mol K is assigned to the saturated liquid state at the normal boiling point (T = 243.74 K).

Figures:

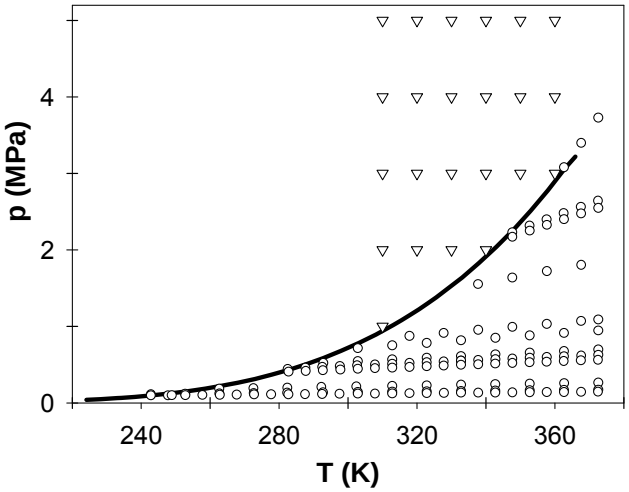

Figure 1.

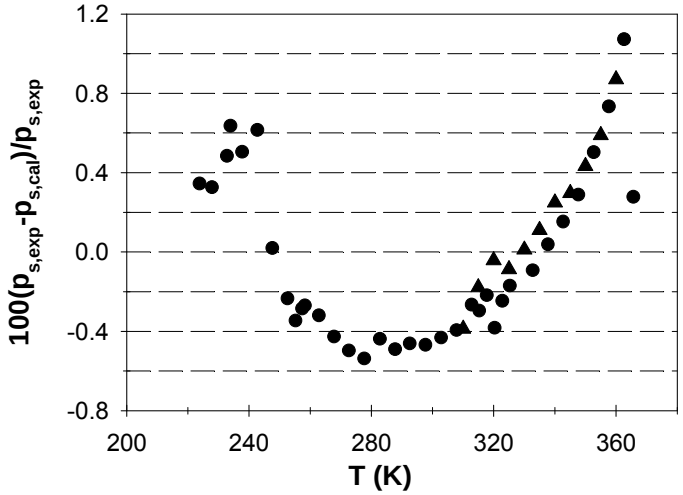

Figure 2.

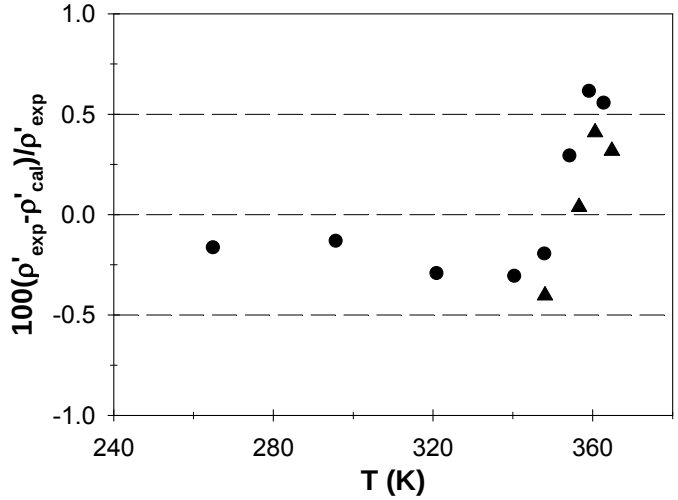

Figure 3.

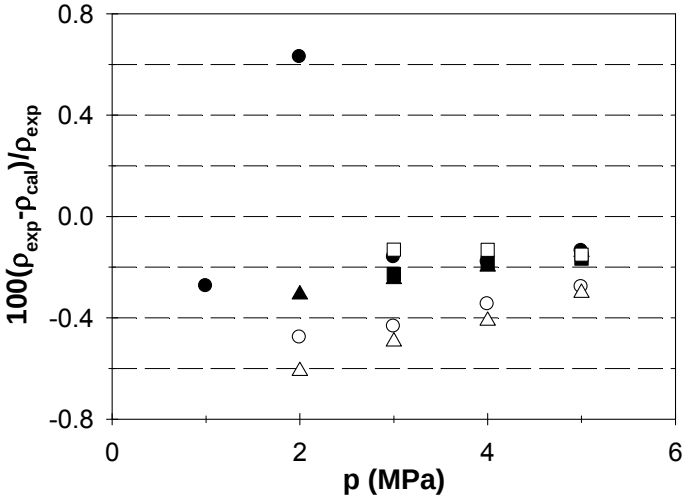

Figure 4.

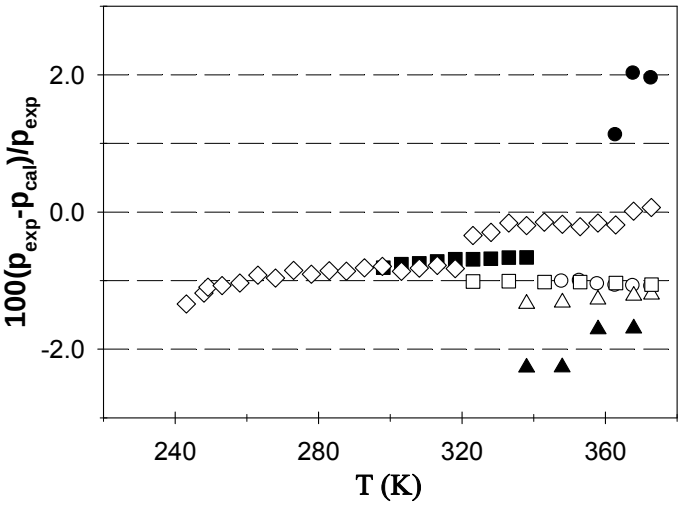

Figure 5.

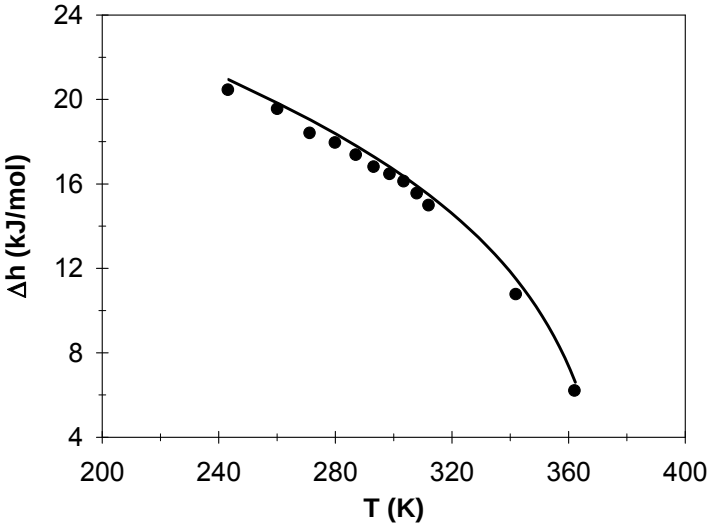

Figure 6.

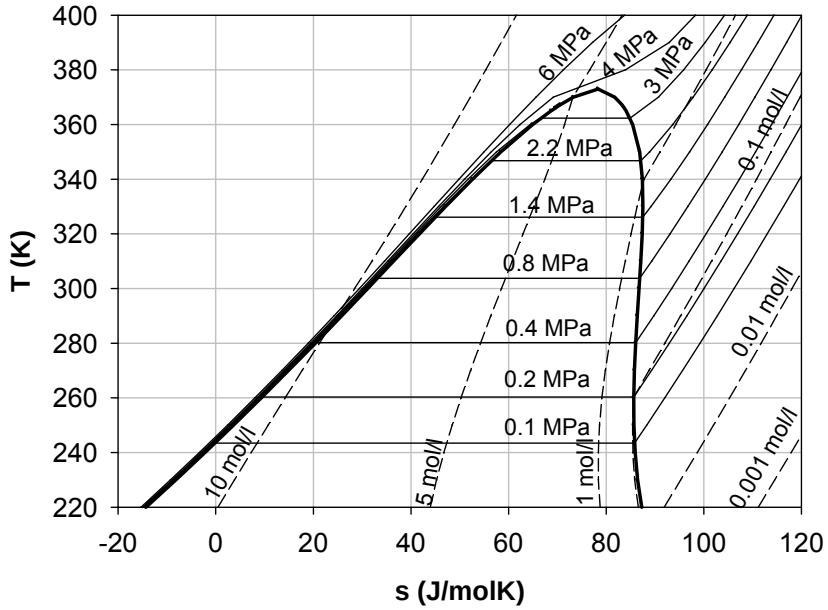
400
380
360
340
320
300
280
260
240
220
T (K)
-20
0
20
40
60
80
100
120
s (J/molK)
6 MPa
4 MPa
3 MPa
2.2 MPa
1.4 MPa
0.8 MPa
0.4 MPa
0.2 MPa
0.1 MPa
10 mol/l
5 mol/l
1 mol/l
0,1 mol/l
0,01 mol/l
0,001 mol/l

Figure 7.

Tables:

Table 1. Experimental critical data of HFO-1234yf

T_c (K)	p_c (MPa)	ρ_c (mol/dm^3)	Source
367.85	3.3820	4.1915	[11]
367.85	3.3749	4.1908	[12]
367.95	3.3820	4.1911	[13]

Table 2. Experimental vapour pressures: temperature ranges, pressure ranges, relative uncertainties, numbers of data points, and sources.

T_{min} (K)	T_{max} (K)	$p_{s,min}$ (MPa)	$p_{s,max}$(MPa)	$\Delta p_s/ p_s$(%)	No. of points	Source
310.00	360.00	0.9397	2.8938	< 0.11	11	[11]
224.12	365.93	0.0389	3.2184	0.25	35	[16]
240.75	353.03	0.0880	2.4476	> 0.25	12	[14]

Table 3. Experimental saturated liquid densities: temperature ranges, saturated liquid density ranges, relative deviations, numbers of data points, and sources.

T_{min} (K)	T_{max} (K)	ρ'_{min} (mol/l)	ρ'_{max} (mol/l)	$\Delta\rho'/\rho'$ (%)	No. of points	Source
348.05	367.85	3.8372	7.4376	<0.36	11	[11]
265.09	365.49	5.6962	10.5260	<0.03	9	[14]

Table 4. Experimental pvT data: temperature ranges, pressure ranges, saturated liquid density ranges, numbers of data points, states, and sources.

T_{min} (K)	T_{max} (K)	p_{min} (MPa)	p_{max} (MPa)	ρ_{min} (mol/l)	ρ_{max}(mol/l)	No. of points	State	Source
243.08	372.82	0.0845	3.7159	0.0437	3.9841	136	vapour	[13]
310.00	360.00	1.0000	5.0000	6.5932	9.4755	23	liquid	[15]

Table 5. Experimental isobaric heat capacities in the liquid: temperature range, heat capacity range, number of data points, and source.

T_{min} (K)	T_{max} (K)	p_{min} (MPa)	p_{max} (MPa)	$c_{p,min}$ (J/molK)	$c_{p,max}$ (J/molK)	No. of points	Source
310	360	2.0	5.0	152.8	297.6	22	[15]

Table 6. Experimental enthalpies: pressure ranges, enthalpy ranges, numbers of data points, states, and sources.

p_{min} (MPa)	p_{max} (MPa)	h_{min} (J/mol)	h_{max} (J/mol)	No. of points	State	Source
0.1	3.0	39002	44932	12	saturated vapour	[17]
0.1	3.0	18589	38318	12	saturated liquid	[17]

Table 7. Isobaric ideal gas heat capacities. Results from the experiments of Kano et al. [41] are compared with quantum mechanical calulations of Hulse et al. [14], Leck [12] and Raabe and Maginn [43] indicating relative deviations.

T (K)	c_p^0 [41] (J/mol K) (1)	c_p^0 [14] (J/mol K) (2)	[(1)-(2)]/(1)	c_p^0 [12] (J/mol K) (3)	[(1)-(3)]/(1)	c_p^0 [43] (J/mol K) (4)	[(1)-(4)]/(1)
273.15	96.09	96.60	-0.53%	93.42	2.86%	86.74	10.8%
298.15	101.55	102.58	-1.00%	98.96	2.62%	92.49	9.8%
310.00	104.05	105.26	-1.15%	101.49	2.52%	95.10	9.4%
353.15	112.64	114.42	-1.56%	110.20	2.21%	----	

Table 8. Comparison of the 4-parameter BACKONE EOS and the 5-parameter BACKONE EOS.

Parameter	4-parameter EOS	5-parameter EOS	Mode
T_0	348.417	347.298	-
ρ_0	4.09179	4.06350	-
α	1.41458	1.41015	-
Q^{*2}	2.76669	2.71832	-
μ^{*2}	-	0.76148	-
AAD of p_s	0.16%	0.31%	fit
AAD of ρ'	0.37%	0.38%	fit
AAD of liquid densities	0.29%	0.28%	predict
AAD of gas pressures	0.99%	0.95%	predict

Table 9. Comparison of calculated with experimental [15] isobaric heat capacities in the liquid. The second column shows the isobaric ideal gas heat capacities c_p^0 [41].

T (K)	$c_p^0{}_{exp}$ (J/mol K)	p (MPa)	$c_{p,exp}$(J/mol K)	$c_{p,cal}$(J/mol K) from $c_p^0{}_{exp}$
310	104	5.00	154 ± 8	160
310		4.00	153 ± 8	161
310		3.00	162 ± 9	163
310		2.00	165 ± 9	165
320	106	5.00	157± 8	164
320		4.00	161± 9	166
320		3.00	168± 9	169
320		2.00	173± 9	172
330	108	5.00	163± 9	170
330		4.00	164± 9	173
330		3.00	179± 9	177
330		2.00	186± 10	183
340	110	5.00	170± 9	177
340		4.00	178±9	183
340		3.00	187± 10	190
340		2.00	205± 10	203
350	112	5.00	182±9	187
350		4.00	196± 10	197
350		3.00	218± 11	215
360	114	5.00	197± 10	202
360		4.00	222± 11	223
360		3.00	297 ± 16	304

Table 10. Vapour pressures, saturated densities, saturated enthalpies, and saturated entropies of HFO-1234yf from BACKONE EOS and c_p^0 from [41].

T (K)	p (MPa)	ρ' (mol/l)	ρ'' (mol/l)	h' (J/mol)	h'' (J/mol)	s' (J/mol K)	s'' (J/mol K)
220	3.086E-02	11.698	0.0172	-3317	19032	-14.29	87.30
225	4.065E-02	11.576	0.0222	-2631	19427	-11.21	86.83
230	5.278E-02	11.452	0.0283	-1938	19823	-8.16	86.45
235	6.763E-02	11.327	0.0357	-1238	20220	-5.16	86.15
240	8.560E-02	11.201	0.0445	-532	20617	-2.19	85.93
245	1.071E-01	11.073	0.0549	181	21015	0.74	85.77
250	1.327E-01	10.944	0.0671	900	21411	3.64	85.68
255	1.627E-01	10.813	0.0813	1627	21807	6.50	85.64
260	1.977E-01	10.681	0.0978	2360	22201	9.34	85.65
265	2.381E-01	10.546	0.1167	3100	22592	12.14	85.70
270	2.847E-01	10.410	0.1384	3847	22980	14.92	85.78
275	3.377E-01	10.271	0.1632	4602	23364	17.67	85.89
280	3.980E-01	10.129	0.1913	5365	23743	20.40	86.03
285	4.659E-01	9.985	0.2232	6137	24116	23.11	86.19
290	5.422E-01	9.837	0.2593	6918	24483	25.80	86.36
295	6.275E-01	9.685	0.3001	7709	24841	28.47	86.55
300	7.223E-01	9.528	0.3461	8511	25190	31.13	86.73
305	8.273E-01	9.366	0.398	9325	25528	33.79	86.91
310	9.433E-01	9.197	0.4565	10152	25853	36.44	87.08
315	1.071E+00	9.021	0.5228	10995	26163	39.09	87.24
320	1.211E+00	8.835	0.5979	11854	26455	41.74	87.37
325	1.364E+00	8.638	0.6834	12732	26726	44.41	87.47
330	1.531E+00	8.427	0.7813	13633	26970	47.11	87.52
335	1.712E+00	8.198	0.8943	14562	27184	49.83	87.51
340	1.909E+00	7.945	1.0261	15524	27357	52.61	87.41
345	2.122E+00	7.661	1.1819	16529	27481	55.46	87.21
350	2.353E+00	7.333	1.3698	17590	27539	58.43	86.86
355	2.602E+00	6.942	1.6028	18729	27508	61.56	86.29
360	2.869E+00	6.455	1.9033	19979	27351	64.95	85.42
365	3.154E+00	5.828	2.3169	21396	26998	68.73	84.08

Table 11. Enthalpies, entropies, and specific volumes of HFO-1234yf at different temperatures and pressures as obtained from BACKONE EOS and c_p^0 from [41].

T (K)	p (MPa)	0.01	0.05	0.1	0.5	1	5	10
220	h (J/mol)	19106	-3316	-3314	-3295	-3272	-3083	-2839
	s (J/mol K)	96.92	-14.29	-14.30	-14.37	-14.46	-15.14	-15.95
	v (dm^3/mol)	181.9	0.085	0.085	0.085	0.085	0.085	0.084
240	h (J/mol)	20835	20722	-531	-515	-495	-326	-105
	s (J/mol K)	104.4	90.72	-2.20	-2.28	-2.38	-3.15	-4.06
	v (dm^3/mol)	198.8	39.10	0.089	0.089	0.089	0.088	0.087
260	h (J/mol)	22656	22565	22448	2369	2386	2526	2718
	s (J/mol K)	111.7	98.09	92.00	9.26	9.15	8.26	7.24
	v (dm^3/mol)	215.5	42.57	20.94	0.094	0.093	0.092	0.091
280	h (J/mol)	24567	24493	24396	5367	5377	5474	5627
	s (J/molK)	118.8	105.2	99.22	20.37	20.23	19.18	18.01
	v (dm^3/mol)	232.3	46.01	22.72	0.099	0.098	0.097	0.095
300	h (J/mol)	26566	26503	26423	25692	8510	8531	8624
	s (J/mol K)	125.7	112.2	106.2	91.06	31.03	29.73	28.35
	v (dm^3/mol)	249.0	49.42	24.47	4.463	0.105	0.102	0.100
320	h (J/mol)	28649	28595	28526	27924	26972	11731	11722
	s (J/mol K)	132.4	118.9	113.0	98.26	90.25	40.05	38.35
	v (dm^3/mol)	265.7	52.81	26.20	4.884	2.169	0.109	0.105
340	h (J/mol)	30813	30766	30706	30196	29444	15137	14941
	s (J/mol K)	139.0	125.5	119.6	105.1	97.74	50.37	48.10
	v (dm^3/mol)	282.3	56.19	27.92	5.283	2.425	0.118	0.112
360	h (J/mol)	33055	33013	32961	32520	31899	18901	18308
	s (J/mol K)	145.4	131.9	126.0	111.8	104.8	61.12	57.72
	v (dm^3/mol)	299.0	59.56	29.63	5.667	2.656	0.133	0.121
380	h (J/mol)	35372	35335	35288	34902	34373	23434	21847
	s (J/mol K)	151.6	138.2	132.3	118.2	111.4	73.36	67.29
	v (dm^3/mol)	315.7	62.92	31.33	6.042	2.871	0.168	0.132
400	h (J/mol)	37760	37727	37686	37343	36884	30299	25553
	s (J/mol K)	157.8	144.3	138.5	124.5	117.9	90.94	76.79
	v (dm^3/mol)	332.3	66.28	33.02	6.410	3.077	0.316	0.148

Table 12. Vapour pressures, saturated densities, and enthalpies of vapourization as function of the temperature from molecular simulations (MS) [38] and BACKONE (B1). Values in parentheses denote standard deviations of the simulations.

T (K)	$p_{s,MS}$ (MPa)	$p_{s,B1}$ (MPa)	ρ'_{MS} (mol/l)	ρ'_{B1} (mol/l)	ρ''_{MS} (mol/l)	ρ''_{B1} (mol/l)	$\Delta h_{,MS}$ (kJ/mol)	$\Delta h_{,B1}$ (kJ/mol)
244.00	0.111 (0.033)	0.103	11.132 (0.075)	11.099	0.057 (0.018)	0.053	21.92 (0.65)	20.90
253.15	0.141 (0.038)	0.151	10.900 (0.048)	10.862	0.073 (0.021)	0.076	21.35 (0.53)	20.30
263.15	0.208 (0.029)	0.222	10.604 (0.032)	10.596	0.102 (0.015)	0.109	20.51 (0.23)	19.62
273.15	0.325 (0.067)	0.317	10.337 (0.050)	10.322	0.162 (0.040)	0.154	19.62 (0.41)	18.90
283.15	0.456 (0.039)	0.440	10.068 (0.071)	10.039	0.219 (0.021)	0.211	18.88 (0.44)	18.13
293.15	0.596 (0.070)	0.595	9.741 (0.103)	9.741	0.290 (0.042)	0.284	17.95 (0.41)	17.29
303.15	0.792 (0.070)	0.787	9.362 (0.118)	9.426	0.384 (0.044)	0.378	16.85 (0.34)	16.38
313.15	1.022 (0.086)	1.022	9.041 (0.095)	9.087	0.499 (0.053)	0.497	15.94 (0.33)	15.37
323.15	1.331 (0.103)	1.306	8.550 (0.182)	8.712	0.661 (0.068)	0.650	14.56 (0.42)	14.22
333.15	1.755 (0.103)	1.643	8.157 (0.193)	8.285	0.929 (0.086)	0.851	12.98 (0.51)	12.89
343.15	2.095 (0.058)	2.042	7.677 (0.329)	7.771	1.133 (0.021)	1.121	11.62 (0.62)	11.29